E-Journal of Advanced Maintenance Vol.9-2 (2017) 104-111
Japan Society of Maintenology

A Research on Numerical Simulation of ACFM Signals for Nondestructive Inspection of Buried Pipes in Nuclear Power Plants

Xudong Li[a], Shejuan Xie[a], Hongwei Yuan[a], Zhenmao Chen[a*] and Toshiyuki Takagi[b]

[a]*Shaanxi Engineering Research Center of NDT and Structure Integrity Evaluation, State Key Laboratory for Strength and Vibration of Mechanical Structures, Xi'an Jiaotong University, 28 West Xianning Road, Xi'an, 710049, China.*
[b]*Innovative Energy Research Center, Institute of Fluid Science, Tohoku University, Aoba-ku, Sendai 980-8577, Japan*

ABSTRACT

Buried pipes in nuclear power plants (NPPs) service in complex environments. Failure in these pipes may result in severe consequences, so that non-destructive testing (NDT) of buried pipes in NPPs is of great importance. Alternating current field measurement (ACFM) method is a potential approach to detect failure in buried pipes due to its advantages such as non-contacting measurement and possible to be applied to long pipes. To evaluate the performance of ACFM for buried pipes, a numerical method and a simulation code are proposed and developed in this paper to calculate the current distribution in a conductive object due to both alternative conduction current injection as well as those induced by the alternative magnetic field due to non-steady current. Comparisons between the current density and related magnetic field results in an elongated plate with cracks obtained by using the developed numerical code and the ANSYS software demonstrated the validity of the proposed numerical method. By using the developed numerical code, dependences of ACFM signals on the lift-off, crack depth, and excitation frequency are simulated and analyzed aiming to improve the ACFM testing conditions for the buried pipe inspection.

KEYWORDS

ACFM, buried pipes, nuclear power plants, numerical simulation, FEM-BEM code

ARTICLE INFORMATION

Article history:
Received 7 Novemver 2016
Accepted 27 April 2017

1. Introduction

Nuclear power plants (NPPs) have many kilometers of buried pipes. Failure in these pipes due to corrosion or ground displacement etc. may result in force outages, costly repairs and could cause personal injuries. For instance, damage of the pipes used in an underground fire protection system in an NPP during the Niigata-ken Chuetsu-oki earthquake presented a realistic threat to the water supply required for firefighting [1]. Thus, nondestructive inspection of the buried pipes in an NPP to ensure their integrity is of great importance. The inspection methods for buried pipes are usually based on visual testing (VT) or other non-destructive testing (NDT) methods [2]. Internal VT cannot be adopted unless the pipes can be drained a prior. However, in an NPP, most of the critical systems requiring inspection cannot be taken out of service, so that VT can hardly be implemented in most cases. Direct manual inspection needs excavations and to remove/replace protective coating, which requires considerable maintenance costs. Even in some cases, pipes are buried under the concrete roadway, which generally complicates the excavation process. In comparison, alternating current field measurement (ACFM) method as one of the NDT methods is considered as a potential way to inspect buried pipes in NPPs. A sensing probe is involved in this method to detect the magnetic field above a conductive object injected with conduction currents [3]. The output signal will be perturbed when the sensing probe scans above the defected area so that the location and dimensions of the defect are possibly to be detected. The sensing probe is not necessary contacting with the inspection object so

*Corresponding author, E-mail: chenzm@mail.xjtu.edu.cn

that large-scale excavation and coating removal can be avoided. Only a limited portion of the buried pipes has to be exposed to inject conduction current, which can save enormous maintenance cost. To evaluate the detectability of ACFM and to optimize the inspection probe and system, a numerical simulation method and code are of great importance for its application in NDT of buried pipes.

In this paper, a numerical method for simulation of ACFM signals is proposed based on the $\boldsymbol{A}$-ϕ formulation and the conventional FEM-BEM hybrid method to calculate the current density in a conductive object under conduction current injection as well as the induction of excitation magnetic field. Second, the numerical method is implemented and validated through comparison of the results of the developed numerical code and those of the ANSYS software. Finally, the numerical code is applied to analysis the influence of liftoff distance, defect size, and excitation frequency on the ACFM signals aiming to improve its detectability for buried tube inspection.

2. Methods

The ACFM problem is basically a combination of eddy current problem and conduction current problem, i.e., a coupling problem of circuit and field. The current inside the material is due to the current conduction and the eddy current due to the alternative magnetic field due to the conduction current. Supposing that the current injection source $\boldsymbol{J}_s$ is a sinusoidal current of low frequency, the governing equations for ACFM problem in conductor region Ω_c can be described by the $\boldsymbol{A}$-ϕ formulation with Coulomb gauge as

$$\frac{1}{\mu}\nabla^2\boldsymbol{A} = \sigma\left(\frac{\partial \boldsymbol{A}}{\partial t} + \nabla\phi\right) \qquad \text{in } \Omega_c \tag{1}$$

$$\nabla\cdot\sigma\left(\frac{\partial \boldsymbol{A}}{\partial t} + \nabla\phi\right) = 0 \qquad \text{in } \Omega_c\ , \tag{2}$$

where $\boldsymbol{A}$ and ϕ are respectively the vector potential and scalar potential; σ and μ are the electric conductivity and magnetic permeability. In case that there is no current source in the air area Ω_a, the electromagnetic fields in the region obeys

$$\frac{1}{\mu}\nabla^2\boldsymbol{A} = 0 \qquad \text{in } \Omega_a\,. \tag{3}$$

On the boundary between the conductor and the air area, the continuity conditions for the normal component of magnetic flux density is satisfied automatically in finite element method (FEM) because vector potential $\boldsymbol{A}$ is continuous on both sides of the finite element interface. The boundary conditions for the tangential component of the magnetic flux density can be described as

$$\frac{\partial \boldsymbol{A}_1}{\partial n} = \frac{\partial \boldsymbol{A}_2}{\partial n}. \tag{4}$$

for nonmagnetic material. In Eq.(4), subscript 1 and 2 denote the variables in the conductor and air area respectively, $\boldsymbol{n}$ is the unit normal vector directed by the conductor to the air area. The current continuity conditions on the boundary surface can be described as

$$\boldsymbol{J}_1\cdot\boldsymbol{n} = \boldsymbol{J}_s\cdot\boldsymbol{n}\,, \tag{5}$$

where $\boldsymbol{J}_1$ and $\boldsymbol{J}_s$ are the current density in conductor and the injected conduction current density respectively.

The governing equations of conductor can be discretized by using FEM. To satisfied the current continuity boundary condition Eq. (5), a special treatment has to be taken during the discretization process of Eq. (2) to cope with the current injection, i.e.,

$$\begin{aligned}
&\sum_{\text{All}}\int_{\Omega_e}[N]^{\mathrm{T}}\nabla\cdot\sigma\left(\frac{\partial \boldsymbol{A}}{\partial t} + \nabla\phi\right)\mathrm{d}\Omega_e \\
&= \sum_{\text{All}}\int_{\Omega_e}\nabla\left\{[N]^{\mathrm{T}}\sigma\left(\frac{\partial \boldsymbol{A}}{\partial t} + \nabla\phi\right)\right\}\mathrm{d}\Omega_e - \sum_{\text{All}}\int_{\Omega_e}\nabla[N]^{\mathrm{T}}\cdot\sigma\left(\frac{\partial \boldsymbol{A}}{\partial t} + \nabla\phi\right)\mathrm{d}\Omega_e \\
&= \sum_{\text{All}}\int_{\Gamma_e}[N]^{\mathrm{T}}\sigma\left(\frac{\partial \boldsymbol{A}}{\partial t} + \nabla\phi\right)\cdot\boldsymbol{n}\,\mathrm{d}\Gamma_e - \sum_{\text{All}}\int_{\Omega_e}\nabla[N]^{\mathrm{T}}\cdot\sigma\left(\frac{\partial \boldsymbol{A}}{\partial t} + \nabla\phi\right)\mathrm{d}\Omega_e\,,
\end{aligned} \tag{6}$$

where $[N]$ is the Lagrange shape function matrix of eight-node isoparametric element; Ω_e and Γ_e respect the volume and the surface of an element in conductor respectively. Excitation conduction current is assumed to be injected into the conductor at given nodes, where $-\boldsymbol{J}\cdot\boldsymbol{n}\,\mathrm{d}\Gamma=I$ with I is the amplitude of the total excitation conduction current. Thus, the first term in the right hand of Eq. (6) can be rewritten as

$$\sum_{\mathrm{All}}\int_{\Gamma_e}[N]^{\mathrm{T}}\sigma\left(\frac{\partial \boldsymbol{A}}{\partial t}+\nabla\varphi\right)\cdot\boldsymbol{n}\,\mathrm{d}\Gamma_e=\sum_{\mathrm{All}}\int_{\Gamma_e}[N]^{\mathrm{T}}\left(-\boldsymbol{J}\cdot\boldsymbol{n}\right)\mathrm{d}\Gamma_e=\sum_{\mathrm{All}}[N_*]^{\mathrm{T}}I=\{f_I\}, \tag{7}$$

where $[N_*]^{\mathrm{T}}$ is a column vector obtained by setting local coordinates of the loading nodes to $[N]^{\mathrm{T}}$, and $\{f_I\}$ is the loading current column vector.

The governing equations of air area can be discretized by using boundary element like what adopted in the FEM-BEM hybrid method [9-11] which enables the current sources in air region not to be meshed. By merging FEM equations and BEM equations together through boundary condition (4), the system of linear equations for ACFM problem can be obtained as

$$\left([P]+[K]\right)\begin{Bmatrix}A_d\\ \Phi\end{Bmatrix}+\left([Q]+[R]\right)\begin{Bmatrix}\partial A_d/\partial t\\ \partial\Phi/\partial t\end{Bmatrix}=\begin{Bmatrix}0\\ f_I\end{Bmatrix}, \tag{8}$$

where $[P]$, $[K]$, $[Q]$, $[R]$ are the FEM and BEM coefficient matrices; $\{A_d\}=\{A_x\ A_y\ A_z\}^{\mathrm{T}}$ and Φ is the time integral of scalar potential ϕ, which is introduced to make the coefficient matrices being symmetry. In this paper, as the time variation is assumed a sinusoidal wave of angular frequency ω, the complex notation can be adopted and the Eq. (8) can be simplified to

$$\left([P]+[K]+j\omega[Q]+j\omega[R]\right)\begin{Bmatrix}\bar{A}_d\\ \bar{\Phi}\end{Bmatrix}=\begin{Bmatrix}0\\ \bar{f}_I\end{Bmatrix}, \tag{9}$$

where $\bar{A}_d$, $\bar{\Phi}$ and $\bar{f}_I$ are the amplitude of A_d, Φ and f_I respectively.

There are four degrees of freedom (DOFs) of vector and scalar potentials on each FEM node and all the DOFs can be obtained by solving the Eq. (9). The current density at each node can be calculated by using

$$\bar{\boldsymbol{J}}=-j\omega\sigma\left([N]\{\bar{\boldsymbol{A}}\}+\nabla[N]\{\bar{\Phi}\}\right). \tag{10}$$

The magnetic flux density at any position in the surrounding space of the conductor can be calculated with the Biot-Savart law as

$$\bar{\boldsymbol{B}}=\frac{\mu_0}{4\pi}\sum_{\mathrm{All}}\int_{\Omega_e}\frac{\bar{\boldsymbol{J}}\times\boldsymbol{e_R}}{R^2}\,\mathrm{d}\Omega_e\,. \tag{11}$$

Following the formulae above, a numerical simulation code is developed based on the conventional FEM-BEM code for eddy current testing problem [9]. Due to the introduction of the BEM, the element subdivision of the air area is avoided, so that the total number of the FEM mesh can be significantly reduced, which saves considerable pretreatment time. The outputs of the code are set as $\bar{\boldsymbol{J}}$ and $\bar{\boldsymbol{B}}$ to know the ACFM signals and to investigate the current distribution inside the material aiming to the optimization of the ACFM method for buried tube problem.

3. Verification of method and numerical code

An elongated rectangular conductor plate of 500×100×10 mm^3 size with a through slit defect of 5×60×10 mm^3 size in the center, as shown in Fig. 1, is adopted as a simplified model of the buried pipes as example to validate the numerical method and corresponding numerical code. The conductivity and relative permeability of the plate material are set as 1.4 MS/m and 1.0 respectively. The plate is subdivided to an FEM mesh of 7000 (70×25×4) hexahedron elements with 9230 nodes and 36920 DOFs. Sinusoidal current of 50 A of frequency of 3 kHz is injected into the plate from both Point 1 and Point 2 at the one end of the long plate, and flows out from the plate at both Point 3 and Point 4 at another end of the long plate. Both of the current density in the plate and the magnetic flux density in the air area are calculated by using the developed code and compared with the results obtained by using the same numerical model but with the ANSYS commercial software.

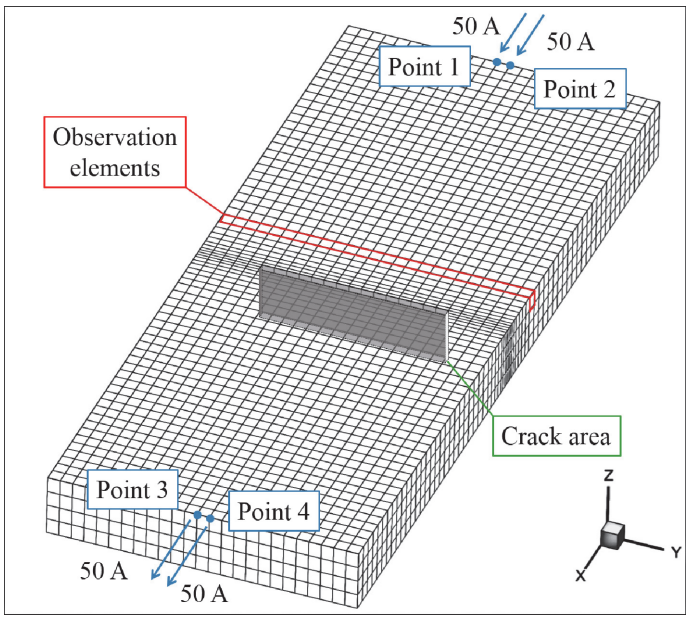

Fig. 1 The model of the conductor plate with through crack

3.1. Results of current density $\bar{J}$

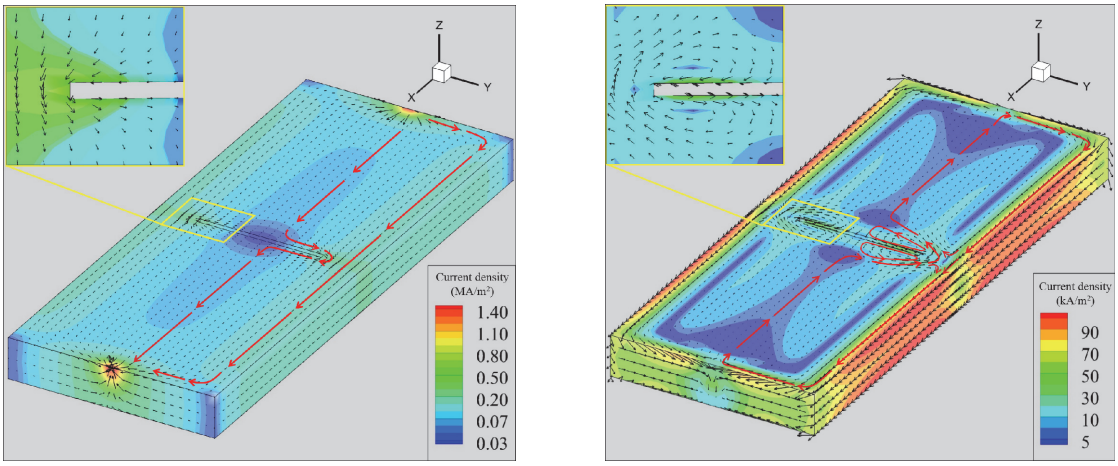

(a) Real part **(b) Imaginary part**

Fig. 2 Current density in the plate

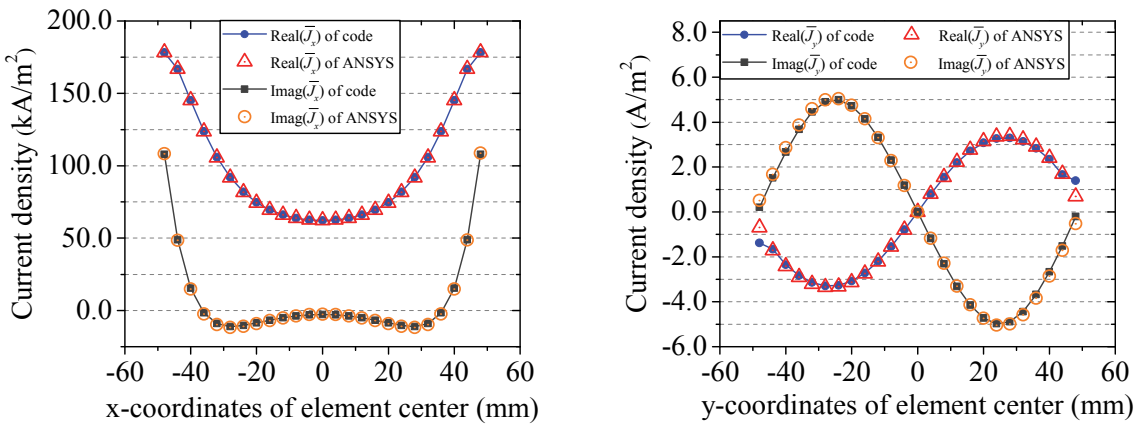

(a) x-component **(b) y-component**

Fig. 3 Results of current density at selected observation elements

The distributions of the current density in the plate obtained by the developed simulation code are shown in Fig. 2, where the red lines with arrow denote the flow direction of total current. To verify the results of present code, the current at an arbitrary row of observation elements as shown in Fig.1 are illustrated in the Fig.3. In Fig.3, the results at the same conditions of the ANSYS software are also presented for comparison. In order to quantitatively compare accuracies between the code and ANSYS results, the normalized root mean squared deviations (NRMSDs) are shown in Table 1. The very good agreement between the two results verifies the validity of the proposed numerical method and corresponding numerical code.

Table 1 Average relative differences between the code and ANSYS results of current density

	Real($\overline{J_x}$)	Imag($\overline{J_x}$)	Real($\overline{J_y}$)	Imag($\overline{J_y}$)
Average relative differences (%)	0.11	0.42	3.02	1.34

3.2. Results of magnetic flux density $\overline{\boldsymbol{B}}$ in the air region

Figure 4 shows the distribution of differential signals (difference of magnetic field signals with and without the defect) of the magnetic flux density in a square plane region 10 mm above the plate and of 200×200 mm^2 size. It can be seen that the magnetic field signals vitiate significantly near the crack tips that means the slit defect can be clearly detected. The comparison, taking the x-component of magnetic field for example, between the differential signals at the scanning line 10 mm above the left crack tip and perpendicular to the crack length obtained by the present numerical code and the ANSYS software is shown in Fig. 5. The NRMSDs between the real part and imaginary part of these two simulated signals are 0.13% and 0.27% respectively. It shows that these two simulated signals meet very well with each other, which demonstrate the validity of numerical method and code again.

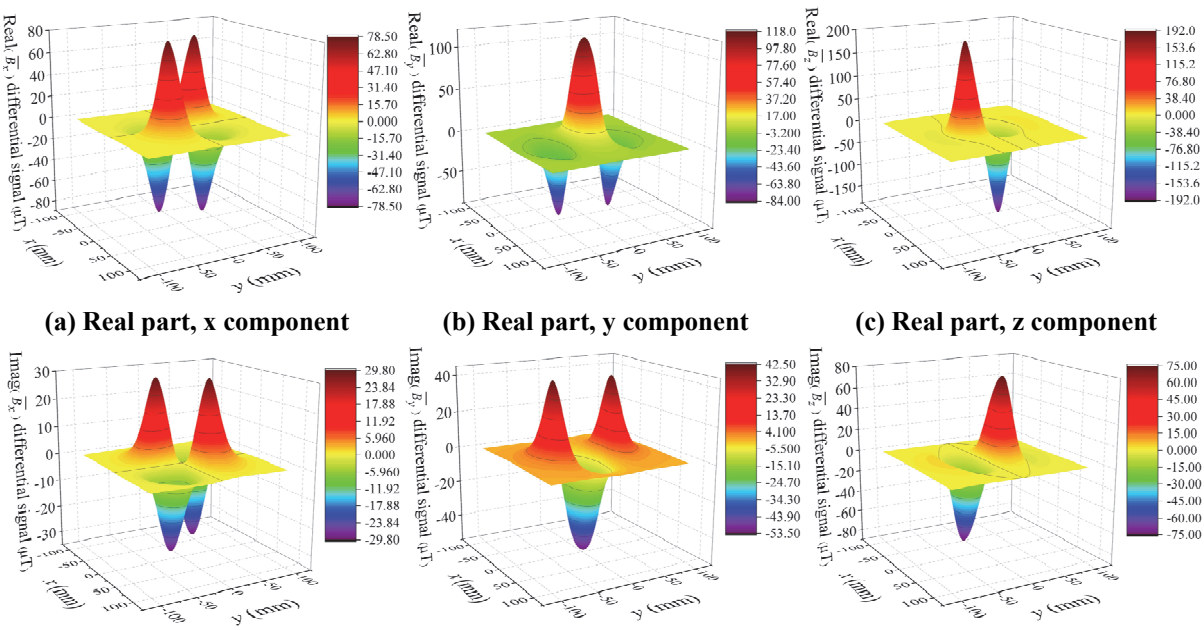

(a) Real part, x component **(b) Real part, y component** **(c) Real part, z component**

(d) Imaginary, x component **(e) Imaginary, y component** **(f) Imaginary, z component**

Fig. 4 Differential signals at the square plane 10 mm above the plate

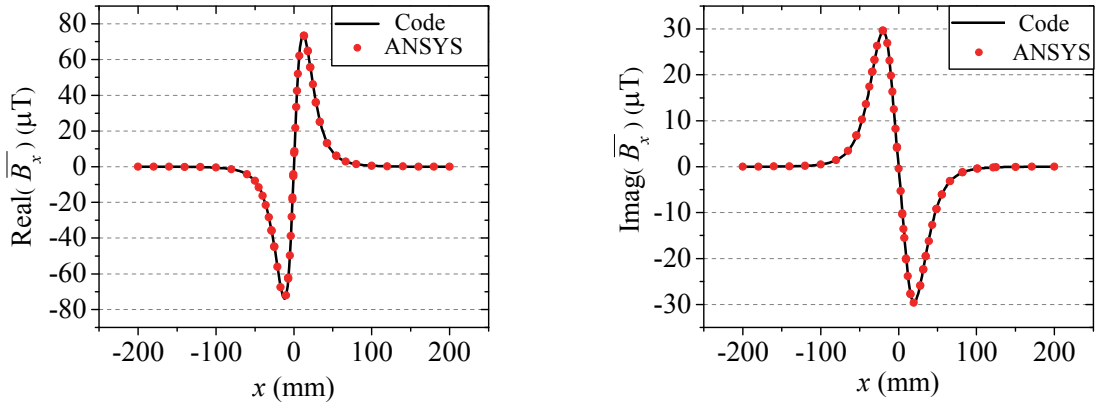

(a) Real part **(b) Imaginary part**

Fig. 5 Differential signals in x-direction above the left crack tip

4. Applications of the code for parameter survey of the ACFM method

Among the differential signals shown in Fig. 4, the x-component is more suitable for defect detection. The first reason is that the magnitude of x-component is relative larger than that of crack free state that makes it easier to be distinguished. Second, the crack length is possible to be estimated easily based on the position information of the signal peaks.

The output signal of ACFM method depends on experimental conditions such as the lift-off distance [4], excitation frequency [6, 7] and the crack depth [5] etc. These factors need to be carefully checked to ensure the ACFM signal including enough defect information in different circumstances.

Same as the ECT problem, the lift-off distance affects the output signal of ACFM significantly. Taking the real part of the magnetic flux density for example, Fig 6(a) shows the evolution of the signal amplitudes at different lift-off distances of magnetic field sensor. It can be seen that the signal intensity is approximately proportional to the negative quadratic of the lift-off distance, which is consistent with the Biot-Savart Law. In addition, the distance between the positions of the two signal peaks increases almost linearly with lift-off distance as shown in Fig 6(b). Hence, in cases of relative large lift-off distance, to enlarge the excitation current or to select a proper excitation frequency may be efficient to enhance the detectability of ACFM method.

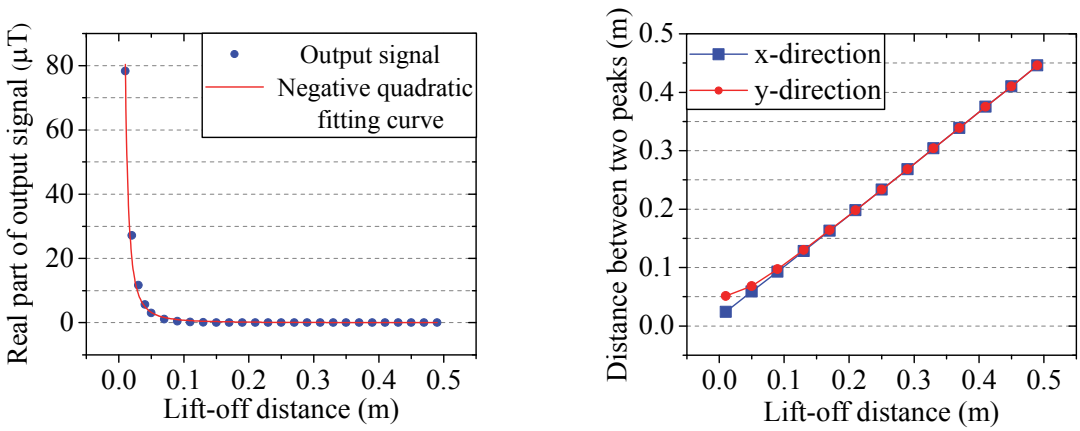

(a) Effect on the intensity **(b) Effect on the distance between two peaks**

Fig. 6 Effects of lift-off distance on the real part of the output signal

Effect of crack depth on the ACFM output signals is as that shown in Fig. 7, where the lift-off distance is fixed to 10 mm and η is defined as the relative crack depth (1 for through crack). The signal increases with crack depth exponentially. In particular, the differential current intensity of through crack is significantly larger than those of non-through cases. This can be intuitively explained based on the current distribution shown in Fig. 8. Current under through crack condition bypasses the

crack from crack tips, and its component in y-direction induces a magnetic flux density component in x-direction above the plate. In contrast, the major current perturbation due to a non-through crack passes under the crack in x-direction, which weakens magnetic flux density component in x-direction.

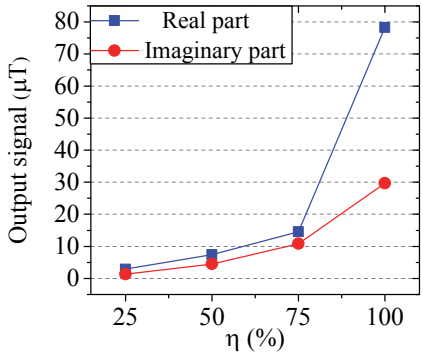

Fig. 7 Effects of crack depth on the output signal

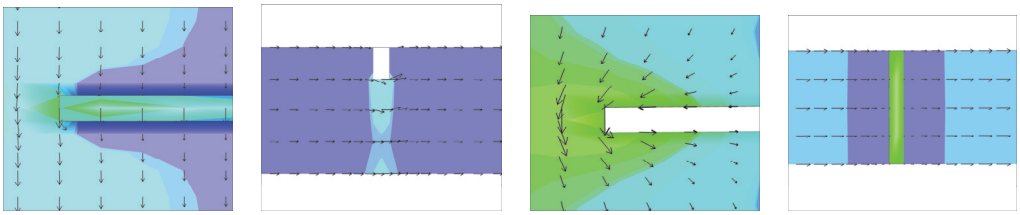

(a) η=0.25, top view (b) η=0.25, y-section view (c) η=1, top view (d) η=1, y-section view

Fig. 8 Real part of current density in plates with cracks of different depth

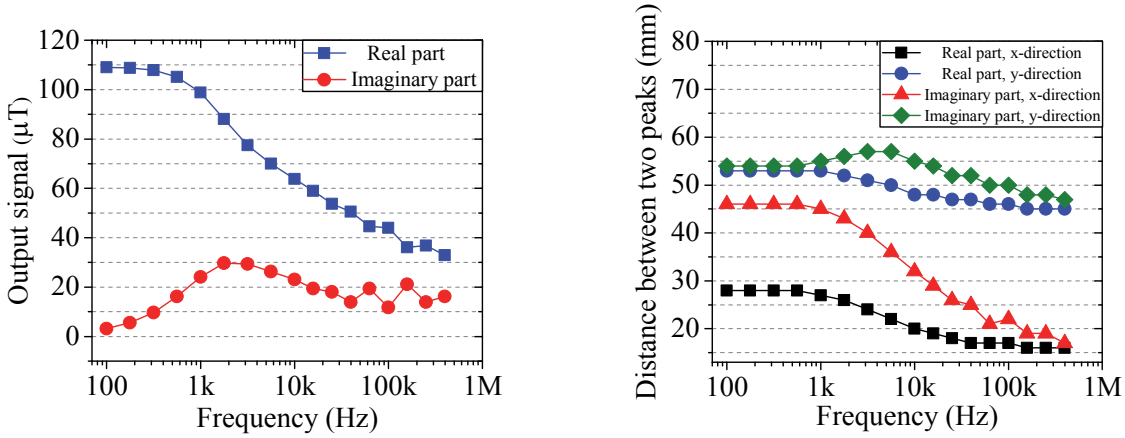

(a) Effect on the intensity (b) Effect on the distance between two peaks

Fig. 9 Effects of excitation frequency on the output signals

On the other hand, the excitation frequency also affects the ACFM output signal significantly, as shown in Fig. 9, where the lift-of distance is 10 mm and η=1. The amplitude of real part magnetic flux density decays with increment of the excitation frequency, while the positioning accuracy is improved in contrast. As for imaginary part of the magnetic field intensity, it increases at first due to the increasing eddy current density, and then decays in a similar way of the real part of the magnetic flux density. When the frequency is higher than about 40 kHz, the imaginary part of ***B*** begins to oscillate due to changes of the distribution of eddy current. Based on results shown in Fig. 9, the real part of the output signal is more suitable for defect detection, and the excitation frequency should be carefully selected to ensure that the output signal is sufficiently strong and the positioning accuracy is sufficiently high.

5. Conclusions

In this paper, a numerical method for simulation of ACFM problem considering a sinusoidal conduction current excitation is proposed and a corresponding simulation code is developed based on the $\boldsymbol{A}$-ϕ formulation and the conventional FEM-BEM hybrid method. The current injection is treated through the current boundary condition. The validity of the proposed numerical method is verified through comparison between simulation results of the present numerical code and the ANSYS commercial software. Finally, effects of lift-off distance, excitation frequency and crack depth on the signals of the ACFM method are investigated by using the developed numerical code aiming to enhance the detectability of the ACFM method for buried pipe inspection.

Acknowledgements

The authors would like to thank the National Magnetic Confinement Fusion Program of China (2013GB113005) and National Natural Science Foundation (51577139 and 51407132) for funding in part. This work was also partly supported by the JSPS Core-to-Core Program, A. Advanced Research Networks “International research core on smart layered materials and structures for energy saving”.

References

[1] Y. Sato, Y. Toyoda, S. Matsuura, et al: "Performance Evaluation on Jointed Pipes Used Underground for Fire Protection at a Nuclear Power Plant as a Response to the Effects of the 2007 Niigata-Ken Chuetsu-Oki Earthquake", ASME 2009 Pressure Vessels and Piping Conference, pp.31-38 (2009).
[2] G. Ogundele, G. Goszczynski, D. Vansligtenhorst: "Inspection of Buried Piping in Nuclear Power Plants: Field Observations and Challenges", ASME 2012 Pressure Vessels and Piping Conference, pp. 257-262 (2012).
[3] M. Lugg, A. Lewis, D. Michael, et al: "The Non-contacting ACFM Technique", Electromagnetic Inspection, a one day meeting of the Materials and Testing Group of the Institute of Physics (1988).
[4] W. Li, G. Chen, X. Yin, et al: "Analysis of the lift-off effect of a U-shaped ACFM system", NDT&E International, 53(2013):31-35.
[5] W. Dover, C. Monahan: "The Measurement of Surface Breaking Cracks by the Electrical Systems ACPD/ACFM", Fatigue & Fracture of Engineering Materials & Structures, 1994, 17(12):1485–1492.
[6] D. Chen, M. Pan, F. Luo: "Research of crack depth detection method based on frequency scanning technique", International Conference on Electronic Measurement and Instruments. 2007:3-751 - 3-754.
[7] W. Li, G. Chen, W. Li, et al: "Analysis of the inducing frequency of a U-shaped ACFM system", NDT&E Int., 44(2011):324-328.
[8] Z. Chen, N. Yusa, K. Miya. “Some advances in numerical analysis techniques for quantitative electromagnetic nondestructive evaluation”. Nondestructive Testing and Evaluation. 24(2009):69–102.
[9] Z. Chen, M. Rebican, K. Miya. “Three-dimensional simulation of remote field ECT using the Ar method and a new formula for signal calculation”. Res Nondestructive Evaluation, 16(2006):35–53.
[10] S. Xie, Z. Chen, T. Takagi, T. Uchimoto. “Quantitative non-destructive evaluation of wall thinning defect in Double-layer pipe of nuclear power plants using pulsed ECT method”. NDT&E Int. 75(2015):87–95.
[11] S. Xie, Z. Chen, T. Takagi, T. Uchimoto. “Development of a very fast simulator for pulsed eddy current testing signals of local wall thinning”. NDT&E Int., 51(2012):45–50.